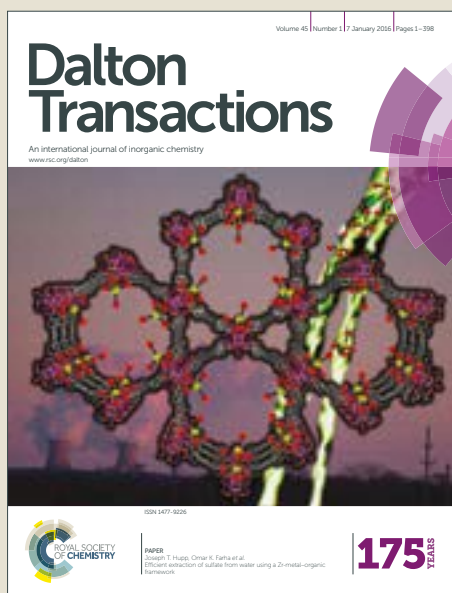


# Dalton Transactions

Accepted Manuscript



This article can be cited before page numbers have been issued, to do this please use: Z. Zhang, Y. Zhou, H. Li, T. Gao and P. Yan, *Dalton Trans.*, 2019, DOI: 10.1039/C9DT00614A.



This is an Accepted Manuscript, which has been through the Royal Society of Chemistry peer review process and has been accepted for publication.

Accepted Manuscripts are published online shortly after acceptance, before technical editing, formatting and proof reading. Using this free service, authors can make their results available to the community, in citable form, before we publish the edited article. We will replace this Accepted Manuscript with the edited and formatted Advance Article as soon as it is available.

You can find more information about Accepted Manuscripts in the [author guidelines](#).

Please note that technical editing may introduce minor changes to the text and/or graphics, which may alter content. The journal's standard [Terms & Conditions](#) and the ethical guidelines, outlined in our [author and reviewer resource centre](#), still apply. In no event shall the Royal Society of Chemistry be held responsible for any errors or omissions in this Accepted Manuscript or any consequences arising from the use of any information it contains.

## Visible light sensitized near-infrared luminescence of ytterbium via ILCT states in quadruple-stranded helicates

Zihan Zhang, Yanyan Zhou, Hongfeng Li,\* Ting Gao and Pengfei Yan\*

 Received 00th January 20xx,  
Accepted 00th January 20xx

DOI: 10.1039/x0xx00000x

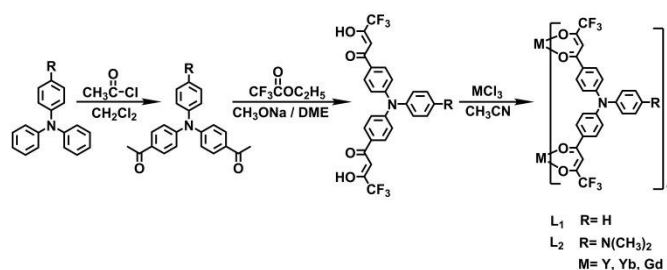
[www.rsc.org/](http://www.rsc.org/)

The visible light excitation is especially important for the NIR emitting materials that are employed in biochemistry and cell biology, since living tissues are generally damaged under UV light irradiation. Here, two new bis- $\beta$ -diketonates,  $L^1$  and  $L^2$  ( $L^1 = 4,4'$ -di(4,4'-trifluoro-1,3-dioxobutyl)-triphenylamine;  $L^2 = 4$ -( $N,N$ -dimethylamino)-4',4''-di(4,4'-trifluoro-1,3-dioxobutyl)-triphenylamine) featuring intra-ligand charge transfer (ILCT) excited state, have been designed and prepared for the synthesis of a series of anionic quadruple-stranded dinuclear helicates ( $(\text{HNEt}_3)_2[\text{M}_2\text{L}^1_4]$  and  $(\text{HNEt}_3)_2[\text{M}_2\text{L}^2_4]$ , where  $M = \text{Yb}$ ,  $\text{Gd}$  and  $\text{Y}$ ). The  $^1\text{H}$  NMR and electrospray mass spectrometry conform the formation of single complexes species in solution. According to the comprehensive spectral characterizations, and in combination with quantum chemical modelling, the ILCT feature of  $L^1$  and  $L^2$  are confirmed. The presence of ILCT allows the use of lower energy excitation wavelength in the visible spectral region to sensitize ytterbium NIR luminescence. In  $(\text{HNEt}_3)_2[\text{Yb}_2\text{L}^1_4]$ , the introduction of strong electron donating  $N,N$ -dimethyl leads to a remarkable red shift of the absorbance edge to 560 nm compared with that in  $(\text{HNEt}_3)_2[\text{Yb}_2\text{L}^2_4]$  at 450 nm. Upon excitation with blue light, the two ytterbium helicates show excellent NIR luminescence in the ranges of 900–1100 nm, with the luminescence quantum yields reach to 1.1% for  $(\text{HNEt}_3)_2[\text{Yb}_2\text{L}^1_4]$  and 1.5% for  $(\text{HNEt}_3)_2[\text{Yb}_2\text{L}^2_4]$  in  $\text{CH}_3\text{CN}$ . Luminescence mechanism experiment show the ILCT singlet path and classic triplet state path together participate in sensitizing  $\text{Yb}(\text{III})$  ions NIR luminescence.

### Introduction

Near-infrared-luminescent lanthanide complexes have potential applications in bioanalysis and cell image areas due to their characteristic line-like emission and long excited state lifetime.<sup>1</sup> Near-infrared luminescence has less photons scatter than visible light emission and can penetrate deep into tissues in biological systems, which can improve detection sensitivity of bioanalysis and biological imaging resolution.<sup>2</sup> The forbidden nature of the f-f transition in trivalent lanthanide ions results in a low absorbance coefficients, and in order to achieve bright emission, a suitable antenna is commonly used to absorb excitation light and transfer energy to the lanthanide centers.<sup>3</sup> However, one of challenges for designing luminescent lanthanide complexes, particularly those aimed at bio-assays and bioimaging, is to shift excitation wavelength from UV to visible range, since living tissues are usually damaged by UV light.<sup>4</sup> Presently, several approaches have been proposed towards this goal, for example excitation through d-block chromophores,<sup>5</sup> by multiphoton excitation,<sup>6</sup> or via triplet states of ligands with low-energy  $\pi-\pi^*$  transition.<sup>7</sup>

Recently, the direct lanthanide sensitization from intra-ligand charge transfer (ILCT) excited state appears as an alternative pathway resulting in a red-shift of excited wavelength far in the visible.<sup>8</sup> For instance, Ouahab et al. have shown that tetrathiafulvalene (TTF) derivatives featuring strong ILCT allowed the use of lower energy excitation wavelength in the visible up to 600 nm for NIR emitters.<sup>9</sup> However, a major drawback of the complexes with ILCT character are their instability in solution resulting from the strong electron-withdrawing groups in the ligands, which could reduce the charge density on the coordinated atoms.<sup>10</sup> This decrease in stability would significantly lower the luminescence quantum yields of lanthanide complexes and limit their applications. Therefore, it is still a challenge to design and synthesize ligands that have strong ILCT character and can form high stable complexes with lanthanide ions.



**Scheme 1** Synthetic routes of  $L^1$ ,  $L^2$ , and their complexes  $(\text{HNEt}_3)_2[\text{M}_2\text{L}^1_4]$  and  $(\text{HNEt}_3)_2[\text{M}_2\text{L}^2_4]$ .

<sup>a</sup> Key Laboratory of Functional Inorganic Material Chemistry, Ministry of Education, P. R. China; School of Chemistry and Materials Science, Heilongjiang University, Harbin 150080, P. R. China. E-mail: lh4612@163.com; yanpf@vip.sina.com

<sup>b</sup> †Electronic Supplementary Information (ESI) available: [details of any supplementary information available should be included here]. See DOI: 10.1039/x0xx00000x

Metal helicates, a model complex of DNA, with two or more metal centres wrapped by two to four ligand strands have been extensively developed due to their glamorous structure and attractively optical, magnetic properties.<sup>11</sup> Piguet has carried out a plenty of work on lanthanide helicates, and revealed that helicates generally show excellent thermodynamic stability in solution.<sup>12</sup> Similarly, several lanthanide dinuclear helicates based on bis- $\beta$ -diketones reported by us also showed higher NIR luminescence quantum yields and relatively large thermodynamic stability in solution.<sup>13</sup>

Herein, two  $C_2$ -symmetric bis- $\beta$ -diketones **L**<sup>1</sup> and **L**<sup>2</sup> are designed for building dinuclear quadruple-stranded helicates with Yb(III) ion, which are comprised of rigid triphenylamine core and two containing strong electron-withdrawing CF<sub>3</sub> substituent 1,3-diketones, respectively. The “push-pull” character in molecules produces low energy ILCT electronic states, where the triphenylamine units acts as an electron donor, and the CF<sub>3</sub> substituent 1,3-diketones as an electron acceptor. As expect, the low energy ILCT states make the lowest energy absorption edges of helicates extend to visible regions at 450 nm for (HNEt<sub>3</sub>)<sub>2</sub>[Yb<sub>2</sub>L<sub>4</sub>], and 560 nm for (HNEt<sub>3</sub>)<sub>2</sub>[Yb<sub>2</sub>L<sub>2</sub>]. Upon excitation with blue light, the helicates show higher luminescence quantum yields, with the QY values are 1.1% for **1** and 1.5% for **2** in CH<sub>3</sub>CN.

## Results and discussion

### Synthesis and characterization of the ligands and complexes

The synthesized procedures of the ligands and their corresponding complexes are outlined in Scheme 1. First, triphenylamine or 4-(N,N-dimethylamino)phenyl diphenylamine are reacted with acetic anhydride using standard Friedel-Crafts reaction to give two diacetyl triphenylamine intermediates, which are then converted to the final ligand **L**<sup>1</sup>, **L**<sup>2</sup> by a traditional Claisen condensation reaction with ethyl trifluoroacetate. <sup>1</sup>H NMR confirm the synthesis and purity of the intermediates and ligands (Figures S1–S4). The Ln(III) quadruple-stranded helicates are obtained by reaction of ligands (**L**<sup>1</sup>, **L**<sup>2</sup>) with the corresponding LnCl<sub>3</sub> salts (Ln = Yb, Gd and Y) in a 2:1 ratio with triethylamine as base. ESI-TOF-MS analysis show corresponding doubly charged peaks for the quadruple-stranded helicates species [Yb<sub>2</sub>L<sub>4</sub>]<sup>2-</sup> or [Yb<sub>2</sub>L<sub>2</sub>]<sup>2-</sup> (Figure 1d). Interestingly, (HNEt<sub>3</sub>)<sub>2</sub>[Yb<sub>2</sub>L<sub>4</sub>] exhibit three clusters of peaks which correspond to three different species with [L – H]<sup>-</sup>, [Yb<sub>2</sub>L<sub>4</sub>]<sup>2-</sup> and [Yb<sub>2</sub>L<sub>4</sub> + H]<sup>-</sup> charge states. The assignments are verified by comparing the corresponding isotopic distributions of the simulated with experimental results. The corresponding yttrium and gadolinium complexes, (HNEt<sub>3</sub>)<sub>2</sub>[Y<sub>2</sub>L<sub>4</sub>] and (HNEt<sub>3</sub>)<sub>2</sub>[Gd<sub>2</sub>L<sub>4</sub>], are also analyzed for comparison (Figure S5–S8). Based on mass spectrometers (ESI-MS) analysis, it confirms the formation of quadruple-stranded helicates with three kinds of lanthanide ions.

To examine the thermodynamic stability and the purity of the complexes in solution, the <sup>1</sup>H NMR spectroscopy are performed on the helicates. Because of the poor resolution of the <sup>1</sup>H NMR for Yb(III) complexes, the isostructural Y(III) complexes are

chosen as substitute for <sup>1</sup>H NMR experiments. As shown in Fig. 1c, only one set of shifted resonances are observed and a total of seven resonances match the C<sub>2</sub> symmetric feature of ligands **L**<sup>1</sup> and **L**<sup>2</sup> and time-averaged C<sub>4</sub> symmetry of complexes **1** and **2** in acetonitrile, respectively. Additionally, the integral area ratios of H in four stranded helicates to two counter cations (protonated triethylamine) also support the formation of quadruple-stranded helicates with the formula of (HNEt<sub>3</sub>)<sub>2</sub>[YL<sub>4</sub>]. Moreover, the absence of resonances of free ligands in the spectra of complexes also reveal the stability and integrity of the helicates on the NMR time scale.

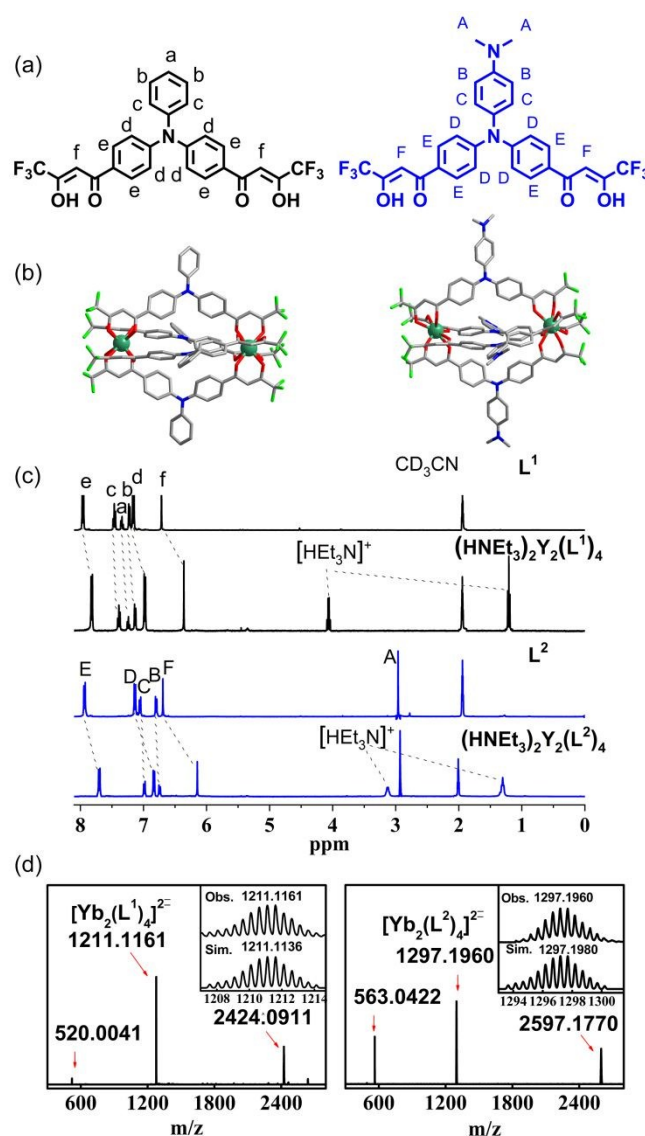


**Fig. 1** Self-assembly of **L**<sup>1</sup>, **L**<sup>2</sup> with LnCl<sub>3</sub>. (a) <sup>1</sup>H NMR assignment of ligands; (b) Sparkle/PM6 ground state geometries of the complexes **1** and **2**; (c) <sup>1</sup>H NMR (400 MHz) spectra of free ligands **L**<sup>1</sup>, **L**<sup>2</sup> and their self-assembled yttrium complexes (HNEt<sub>3</sub>)<sub>2</sub>[Y<sub>2</sub>L<sub>4</sub>] and (HNEt<sub>3</sub>)<sub>2</sub>[Y<sub>2</sub>L<sub>2</sub>] (CD<sub>3</sub>CN); (d) ESI-TOF-MS of helicates **1** and **2** with insets showing the observed (Obs.) and simulated (Sim.) isotopic patterns of the anion [Y<sub>2</sub>L<sub>4</sub>]<sup>2-</sup> peaks.

To obtain better structural insight in this assembly, a molecular model is built with the parameters Sparkle/PM6 using MOPAC 2016 program implemented in the LUMPAC 3.0

software, and this routine converges to the quadruple-stranded helicates shown in Fig. 1b. In a helicate, each  $\text{Yb}^{3+}$  ion is eight-coordinated to O atoms from four  $\beta$ -diketonate ligands. The triphenylamine (TPA) cores adopts propeller-like conformation, resulting in two pendant diketone arms wrap two metal centres forming helical twistification. Due to the absence of chiral element in ligands, both helicate will present as two pairs of racemes with homochiral  $\text{Yb}^{3+}$  centers, either a left-handed  $\Lambda$ ,  $\Lambda$  or right-handed  $\Delta$ ,  $\Delta$  configuration (Fig. S9).

### Electronic Spectroscopy and TD-DFT Calculations

UV-Vis absorption spectra of  $\text{L}^1$  and  $\text{L}^2$  and their corresponding  $\text{Yb}(\text{III})$  complexes in  $\text{CH}_3\text{CN}$  are shown in Fig. 2. The absorption spectra exhibit one broad, intense absorption bands with a maxima at around 390–400 nm and a shoulder peak at about 330 nm. It is noteworthy that the molar extinction coefficient ratios ( $\epsilon_L/\epsilon_H$ ) of low energy band ( $\epsilon_L$ ) to high energy band ( $\epsilon_H$ ) show significant increase from  $\epsilon_L/\epsilon_H = 1.5, 1.2$  in  $\text{L}^1, \text{L}^2$  to 3.0, 1.7 for that in **1** and **2**, respectively. This obvious change indicates that the coordination of  $\text{Ln}(\text{III})$  ions heavily influence electron transition distributions and probabilities in chromophores.

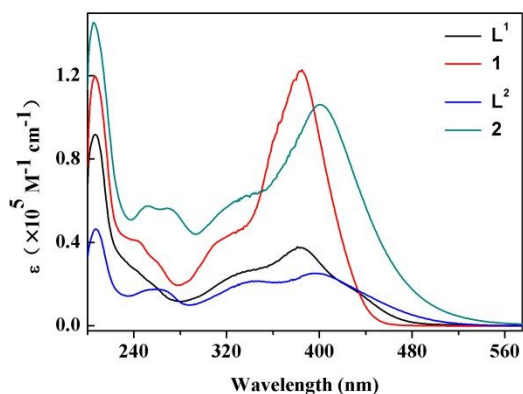


Fig. 2 UV-Vis absorption spectra of  $\text{L}^1, \text{L}^2$  and their corresponding complexes **1** and **2** in  $\text{CH}_3\text{CN}$  ( $c = 1.0 \times 10^{-5}$  M for ligands;  $c = 2.5 \times 10^{-6}$  M for complexes).

To gain further insight into the transition, the corresponding electronic structure calculations using TD-DFT are also performed using the Gaussian 09 package. For comparing with the calculated results, the experimental absorption curves in the range of 280–540 nm have been fitted into three bands by Gaussian deconvolution (Figure S10). The calculated absorption spectra reproduce the experimental curves (Figure S11). A summary of calculation is given in Table 1, and their corresponding molecular orbitals are shown in Fig. 3. According to the calculation, the lowest energy transitions band ( $\lambda = 358$  nm,  $f = 0.2212$  for  $\text{L}^1$ ) is attributed to  $\pi-\pi^*$  charge transfer (CT) corresponding essentially to the HOMO (TPA)  $\rightarrow$  LUMO (DK), HOMO  $- 3 \rightarrow$  LUMO  $+ 1$  transition and intra-diketone  $\pi-\pi^*$  transition HOMO  $- 2$  (DK)  $\rightarrow$  LUMO (DK) (TPA = triphenylamine; DK = diketone units). The HOMO is a  $\pi$  orbital centered on the TPA fragment whereas the LUMO, LUMO  $+ 1$  is centered on the diketone moiety. The next absorption band at 350 nm ( $f = 0.5344$ ) and 318 nm ( $f = 0.2785$ ) are mainly attributed to charge transfer (CT) HOMO  $\rightarrow$  LUMO, HOMO  $\rightarrow$  LUMO  $+ 1$  transition, but with a higher oscillation intensities.

Based on these transition distributions, the low energy transitions are mainly attributed to an intramolecular CT from the donor TPA fragment to the acceptor  $\beta$ -diketone units. Finally, the highest-energy bands at 233 nm and 230 nm are attributed to the  $\pi-\pi^*$  HOMO  $- 6 \rightarrow$  LUMO, HOMO  $- 6 \rightarrow$  LUMO intra-diketone transitions and  $\pi-\pi^*$  HOMO  $\rightarrow$  LUMO  $+ 6$  intra-TPA transitions.

Similar orbitals transitions can also be observed in  $\text{L}^2$  with a strong electron-donor N,N-dimethyl group. The band ( $\lambda = 372$  nm,  $f = 0.6718$ ) is attributed to ILCT transition from the  $\pi-\pi^*$  HOMO (N,N-TPA)  $\rightarrow$  LUMO (DK), while the transition ( $\lambda = 330$  nm,  $f = 0.3036$ ) is attributed to HOMO  $\rightarrow$  LUMO  $+ 1$ , HOMO  $\rightarrow$  LUMO CT transitions, respectively. The highest energy bands at  $\lambda = 258$  nm and  $\lambda = 229$  nm are corresponding to the HOMO  $- 7 \rightarrow$  LUMO, HOMO  $- 6 \rightarrow$  LUMO  $+ 1$   $\pi-\pi^*$  transitions in  $\beta$ -diketone moieties. Thus, the theoretical modelling prove that charge transfer does indeed take place between triphenylamine units as an electron donating group and the  $\beta$ -diketone moieties acting as the accepting group.

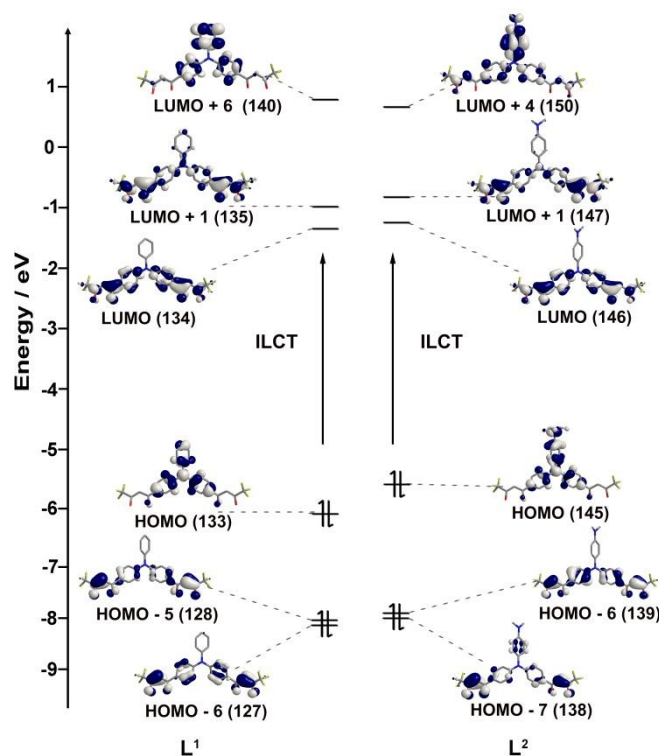


Fig. 3 Molecular orbital diagrams of  $\text{L}^1$  and  $\text{L}^2$ .

Generally, the introduction of intense electron-donating group and/or electron-withdrawing group will facilitate the ILCT transition from donor to acceptor. Compared with the ligands, the absorption bands attributed to ILCT transitions of complexes **1** and **2** show the larger intensity ratios of  $\epsilon_L/\epsilon_H$ , which can be rationalized by Lewis acidity of  $\text{Yb}(\text{III})$  ion. It helps increase electron withdrawing capacity of acceptor. In addition, the strong electron-donor N,N-dimethyl group red-shifts the maximum absorption edges from 440 nm for **1** to 520 nm for **2**.

To further confirm the formation of the ILCT state, the spectral dependence of ligand on solvent polarity is studied,

because intramolecular charge transfer processes usually generate large Stokes' shifts of the emission band in polar solvents.<sup>14</sup> The fluorescence spectra of **L**<sup>1</sup> and **L**<sup>2</sup> show red shifts of 92 nm and 64 nm of emission maximum as solvent polarity increases from n-Hexane to dichloroethane (Figure S12). It is

well known that solvatochromism is the characteristic of an ILCT state. Moreover, a good correlation of ligand luminescence maximum versus Reinhardt's empirical solvent polarity parameter  $E_T(30)$  also indicates the presence of ILCT transition (Figure S13).<sup>15</sup>

**Table 1** Most Important TD-DFT Calculated Excitations Energies Associated with an Oscillator Strength  $f > 0.20$  and Major Assignment of Electronic Transitions of **L**<sup>1</sup> and **L**<sup>2</sup>.

	Exptl. energy (nm)	Calcd. energy (nm)	Oscillator strengths	Location of transition	Assignment	Nature of transitions
<b>L</b> <sup>1</sup>	426	358	0.2212	ILCT	$\pi \rightarrow \pi^*$	HOMO $\rightarrow$ LUMO (0.3465)
				ILCT	$\pi \rightarrow \pi^*$	HOMO - 3 $\rightarrow$ LUMO + 1 (0.2278)
				DK	$\pi \rightarrow \pi^*$	HOMO - 2 $\rightarrow$ LUMO (0.3083)
	382	350	0.5344	ILCT	$\pi \rightarrow \pi^*$	HOMO $\rightarrow$ LUMO (0.6750)
				ILCT	$\pi \rightarrow \pi^*$	HOMO $\rightarrow$ LUMO + 1 (0.9369)
				DK	$\pi \rightarrow \pi^*$	HOMO - 6 $\rightarrow$ LUMO (0.3363)
				TPA	$\pi \rightarrow \pi^*$	HOMO $\rightarrow$ LUMO + 6 (0.2142)
				DK	$\pi \rightarrow \pi^*$	HOMO - 6 $\rightarrow$ LUMO (0.2138)
				ILCT	$\pi \rightarrow \pi^*$	HOMO - 4 $\rightarrow$ LUMO (0.2055)
				DK	$\pi \rightarrow \pi^*$	HOMO - 6 $\rightarrow$ LUMO (0.3363)
268	233	0.3131	ILCT	$\pi \rightarrow \pi^*$	HOMO $\rightarrow$ LUMO (0.2940)	
			ILCT	$\pi \rightarrow \pi^*$	HOMO - 4 $\rightarrow$ LUMO (0.2055)	
<b>L</b> <sup>2</sup>	443	372	0.6719	ILCT	$\pi \rightarrow \pi^*$	HOMO $\rightarrow$ LUMO (0.9643)
				ILCT	$\pi \rightarrow \pi^*$	HOMO $\rightarrow$ LUMO + 1 (0.9672)
				TPA	$\pi \rightarrow \pi^*$	HOMO $\rightarrow$ LUMO + 4 (0.6425)
				DK	$\pi \rightarrow \pi^*$	HOMO - 7 $\rightarrow$ LUMO (0.4963)
				DK	$\pi \rightarrow \pi^*$	HOMO - 6 $\rightarrow$ LUMO + 1 (0.2470)
<b>L</b> <sup>2</sup>	399	330	0.3036	ILCT	$\pi \rightarrow \pi^*$	HOMO $\rightarrow$ LUMO + 1 (0.9672)
				ILCT	$\pi \rightarrow \pi^*$	HOMO $\rightarrow$ LUMO + 1 (0.9672)
				TPA	$\pi \rightarrow \pi^*$	HOMO $\rightarrow$ LUMO + 4 (0.6425)
				DK	$\pi \rightarrow \pi^*$	HOMO - 7 $\rightarrow$ LUMO (0.4963)
<b>L</b> <sup>2</sup>	272	258	0.2424	TPA	$\pi \rightarrow \pi^*$	HOMO $\rightarrow$ LUMO + 4 (0.6425)
				DK	$\pi \rightarrow \pi^*$	HOMO - 7 $\rightarrow$ LUMO (0.4963)
				DK	$\pi \rightarrow \pi^*$	HOMO - 6 $\rightarrow$ LUMO + 1 (0.2470)
<b>L</b> <sup>2</sup>	272	229	0.5635	DK	$\pi \rightarrow \pi^*$	HOMO - 7 $\rightarrow$ LUMO (0.4963)
				DK	$\pi \rightarrow \pi^*$	HOMO - 6 $\rightarrow$ LUMO + 1 (0.2470)
				DK	$\pi \rightarrow \pi^*$	HOMO - 6 $\rightarrow$ LUMO + 1 (0.2470)

### Photoluminescence Properties of Complexes

The NIR-luminescent properties of the Yb(III) complexes are investigated in CH<sub>3</sub>CN at room temperature. The excitation spectra of complexes are recorded by monitoring the maximum emission at 1042 nm (Fig. 4). A broad bands in the range of 300–500 nm with the maxima at about 380 nm and 415 nm are observed, which well match the corresponding absorption spectra confirming that the energy transfer takes place from the ligands to Yb(III) ions. To our delight, most parts of the excitation bands localize in blue light region (420–500 nm) due to the presence of ILCT state in ligands. From the excitation wavelength dependent emission spectra, Yb(III) ion present obvious NIR emission with the excitation wavelength in visible region (Fig. 14). The visible light excitation is especially important for the NIR emitting materials employed in biochemistry and cell biology, since living tissues are sensitive to UV irritation.

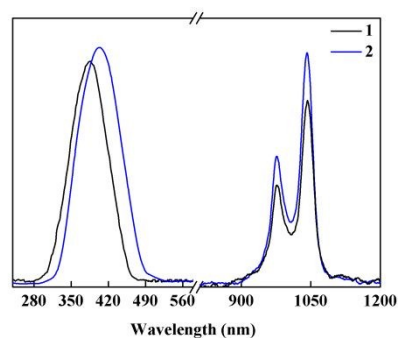


**Fig. 4** Excitation (left) and emission (right) spectra of **1** and **2** in CH<sub>3</sub>CN ( $c = 2.5 \times 10^{-6}$  M; Excitation spectra monitoring the  ${}^2F_{5/2} \rightarrow {}^2F_{7/2}$  transition at 1042 nm).

Upon excitation with the maximum band at 400 nm (Fig. 4), complexes **1** and **2** show the characteristic emission of Yb(III) ions corresponding to the  ${}^2F_{5/2} \rightarrow {}^2F_{7/2}$  transition at 900–1200 nm. Interestingly, two complexes show similar spectra pattern, but different luminescent intensity. Since the spectral splits are related to symmetry of ligand fields,<sup>16</sup> the consistence of the splits indicates the Yb(III) ions in two complexes have similar coordination environment and symmetry.

In the same concentration of complexes in CH<sub>3</sub>CN, the complex **2** displays about 1.3 times higher signal intensity than complex **1**. Taking the Yb(TTA)<sub>3</sub>(H<sub>2</sub>O)<sub>2</sub> as reference,<sup>17</sup> the values of emission quantum yields ( $\Phi_{tot}$ ) of two complexes in CH<sub>3</sub>CN are calculated to be 1.1% for **1** and 1.5% for **2**, respectively. The values are obviously higher than the most of Yb(III) complexes with H-containing ligands.<sup>18</sup> As reported previously by us, the helical structure can effectively depress the nonradiative transition caused by high-energy oscillators in ligands, and saturated eight coordination geometries can also decrease the probability of solvent entering the metal centers.<sup>13b</sup> In luminescent lanthanide complex, the luminescence quantum yield ( $\Phi_{tot}$ ) is determined by two factors: (1) the efficiency of the energy transfer ( $\eta_{ET}$ ); (2) and the intrinsic quantum yield ( $\Phi_{Ln}$ ) of the lanthanide luminescence (eqn. 1)

$$\Phi_{tot} = \eta_{ET} \Phi_{Ln} \quad (1)$$

According to this equation, the large  $\Phi_{tot}$  value of lanthanide center must originate from the improved  $\eta_{ET}$  or  $\Phi_{Ln}$ , or the both. The intrinsic quantum yields of Yb(III) ion luminescence could be estimated using the equation 2, after the calculation of the radiative lifetime ( $\tau_{rad}$ ) from the absorption spectra of Yb(III) ion

in complexes (Figure S15) with a modified Einstein equation (eqn. 3):<sup>19</sup>

$$\Phi_{Ln} = \frac{k_r}{k_r + k_{nr}} = \frac{\tau_{obs}}{\tau_{rad}} \quad (2)$$

$$\frac{1}{\tau_{rad}} = k_r = 2303 \times \frac{8\pi c n^2 \tilde{\nu}_m^2 (2J+1)}{N_A (2J'+1)} \int \varepsilon(\tilde{\nu}) d\tilde{\nu} \quad (3)$$

$$\tilde{\nu}_m = \frac{\int \tilde{\nu} \cdot \varepsilon(\tilde{\nu}) d\tilde{\nu}}{\int \varepsilon(\tilde{\nu}) d\tilde{\nu}}$$

Where,  $N_A$  is Avogadro's number,  $c$  is the speed of light in centimeters per second,  $J$  and  $J'$  are the quantum numbers for the ground and excited states, respectively.  $\int \varepsilon(\tilde{\nu}) d\tilde{\nu}$  is the integrated spectrum of the f-f transition,  $\tilde{\nu}_m$  is the barycenter of the transition, and  $n = 1.3456$  for CH<sub>3</sub>CN solution. In terms of these equations, the radiative lifetime ( $\tau_{rad}$ ) are calculated to be 399  $\mu$ s and 499  $\mu$ s for **1** and **2**, respectively.

The observed lifetimes ( $\tau_{obs}$ ) are determined by monitoring the emission decay curves within the  ${}^2F_{5/2} \rightarrow {}^2F_{7/2}$  transition at 1042 nm. Typical decay profiles of **1** and **2** are shown in Figure S16. The two decay curves are well-reproduced by single-exponential functions, indicating that only one species exists in the excited state of the complexes. The lifetimes of **1** and **2** are found to be 14.7  $\mu$ s and 15.4  $\mu$ s, respectively. While the lifetime values increase to 14.7  $\mu$ s and 15.4  $\mu$ s, following the temperature decrease to 77 K. This could be easily understood because the low temperature decrease nonradiative transition caused by thermal vibration of molecules. With the calculated radiative lifetimes ( $\tau_{rad}$ ) and the observed lifetimes ( $\tau_{obs}$ ), the intrinsic quantum yields ( $\Phi_{Ln}$ , eqn.1) are found to be 3.7% and 3.1% for **1** and **2**, respectively. With the observed and intrinsic quantum yields, the energy transfer efficiencies ( $\eta_{ET}$ , eqn. 1) are found to be 30.6% and 47.6% for **1** and **2**, respectively. From above results, it can be observed that the higher luminescence quantum yield of complex **2** are contributed from the larger sensitised efficiency ( $\eta_{ET2}$ , 47.6% >  $\eta_{ET1}$ , 30.6%), because the intrinsic quantum yields are not much difference between them. In lanthanide luminescence complexes, the energy-level matching between the excited states energy levels of ligands and metal ions are key for realizing effective energy transfer. Several different excited states of chromophores have been exploited for populating the excited states of Ln(III) ions, such as singlet states,<sup>20</sup> triplet states,<sup>21</sup> intra-ligand transfer state (ILCT),<sup>22</sup> and metal-to-ligand charge transfer states (MLCT).<sup>23</sup> The triplet state sensitization is the usual pathway due to the heavy atom effects of lanthanide ions, which will facilitate the intersystem crossing from singlet to triplet state. The triplet state energy levels can be easily estimated from the emission spectra of their Gd(III) complexes at 77 K. Because the lowest excited energy level of Gd<sup>3+</sup> ion ( ${}^6P_{7/2}$ ) is too high to accept energy from ligands, the triplet state energy level of ligand is not significantly affected by the Gd(III) ion. As shown in Figure S17, the complexes (HNET<sub>3</sub>)<sub>2</sub>[Gd<sub>2</sub>L<sup>1</sup><sub>4</sub>] and (HNET<sub>3</sub>)<sub>2</sub>[Gd<sub>2</sub>L<sup>2</sup><sub>4</sub>] display a broad emission bands in the range of 450–720 nm at 77 K. To avoid possible emission from residual fluorescence of ligands, the time-resolution experiments are performed. Upon enforcement

of a time delay (100  $\mu$ s), the high energy bands in 440–500 nm for **1** disappears and is consequently assigned as arising from a  ${}^1\pi\pi^*$  state. After eliminating this interference, the triplet state energy levels  ${}^3\pi\pi^*$  of **L<sup>1</sup>** and **L<sup>2</sup>** are calculated to be 18 587 cm<sup>-1</sup> and 16 313 cm<sup>-1</sup> by referring to their maximum emission wavelengths, which are both higher than the energy level of  ${}^2F_{5/2}$ , 10 250 cm<sup>-1</sup> of Yb(III) ion. The energy gap  $\Delta E$  ( ${}^3\pi\pi^* - {}^2F_{5/2}$ ) is 6063 cm<sup>-1</sup> for **2** and 8337 cm<sup>-1</sup> for **1**. Generally, the lower energy gap is favored to the energy transfer from high energy level to low energy state.<sup>24</sup> Thus, it is rationalized to explain the higher energy transfer efficiency of **2** than that in **1**.

Due to the presence of ILCT state in ligands, the participation of ILCT states in sensitizing Yb(III) ions NIR luminescence are put into consideration. To verify this, the fluorescence spectra of their corresponding Gd(III) complexes are recorded and compared with Yb(III) complexes **1** and **2** (Figure S18). The fluorescent intensities of ligands in Yb(III) complexes show an obvious decreases than that in Gd(III) complexes. Due to the same heavy atom effect and the absence of energy transfer from ligand to Gd(III) ions, the decreases in emitting intensities should attribute to the energy transfer from the ILCT states to  ${}^2F_{5/2}$  energy level of Yb(III) ions. In addition, it can be observed that the decrease of emission intensity in **2** is more obvious than that in **1**. Based on the integration areas of emission peaks, the energy transfer efficiency from  ${}^1\pi\pi^*$  ILCT emission to Yb(III) excited state are estimated to be 28% for **1** and 43% for **2**. The higher energy transfer efficiency for **2** should attribute to the lower ILCT state energy level ( ${}^1\text{ILCT}^*$ , 19 231 cm<sup>-1</sup>) than that for **1** with 22 727 cm<sup>-1</sup>, which are calculated from the maximum wavelengths of UV-Vis absorbance edges of Yb(III) complexes.

On the basis of above experimental results, it can be concluded that the ILCT state and triplet state together participate in energy transfer pathway. The lower energy gap between excited states of ligands (regardless of  ${}^1\text{ILCT}^*$  or  ${}^3\pi\pi^*$ ) and  ${}^2F_{5/2}$  energy level of Yb(III) ion are favored to improve the sensitization efficiency and increase the luminescence quantum yields of lanthanide complexes.

## Conclusions

In summary, two new Yb(III) quadruple-stranded helicates based on bis- $\beta$ -diketone ligand are developed, which show visible light sensitizing NIR luminescence upon excitation with low-lying ILCT states of the ligands. TD-DFT calculation combine with the polarity dependence of emission spectra confirm the ILCT behavior in ligands. The existence of ILCT state red-shift the absorption wavelength to the visible region, especially in the case of **L<sup>2</sup>**, the lowest energy absorption edge further red-shift about 100 nm compared with that in **L<sup>1</sup>** due to the introduction of intense electron donor N,N-dimethyl. Upon excitation with blue light at 420 nm, the two complexes show high luminescence quantum yields of 1.1% for **1** and 1.5% for **2**. The helical structure and saturated eight coordination geometries effectively depress the nonradiative transition caused by high-energy oscillators in ligands, and preventing the solvent as H<sub>2</sub>O from coordinating to metal centers. Luminescence mechanism experiment show the ILCT singlet and classic triplet state paths

are both responsible for sensitizing Yb(III) ions NIR luminescence. The enhanced luminescent quantum yield of **2** is attributed to the larger energy transfer efficiency from ILCT state to metal centers and lower energy gap between  $^3\pi\pi^*$  of **L**<sup>2</sup> and  $^2F_{5/2}$  energy level of Yb(III) ion. In a word, the synthesis of helicate based on ligand featuring intra-ligand charge transfer (ILCT) excited state is a valuable approach for enhancing the lanthanide ions NIR luminescence with visible-light excitation.

## Experimental

### Materials and instruments

The commercially available chemicals are analytical reagent grade and used without further purification.

Elemental analyses were performed on an Elementar Vario EL cube analyzer. The <sup>1</sup>H NMR spectra are recorded on a Bruker Avance III 400 MHz spectrometer. Electron ionization (EI) and Electrospray time-of-flight (ESI-TOF) mass spectra were recorded on Agilent 5975N and Bruker maXis mass spectrometers, respectively. UV-Vis-NIR spectra were recorded on a Perkin-Elmer Lambda 25 spectrometer. Excitation and emission spectra were measured with an Edinburgh FLS 920 fluorescence spectrophotometer. Luminescence lifetimes were recorded on a single photon counting spectrometer from Edinburgh Instrument (FLS 920) with a microsecond pulse lamp as the excitation sources. The data were analyzed by software supplied by Edinburgh Instruments. The luminescence quantum yields of the Yb(III) complexes were measured in CH<sub>3</sub>CN at room temperature and cited relative to a reference solution of [Yb(tta)<sub>3</sub>(H<sub>2</sub>O)<sub>2</sub>] ( $\Phi = 0.35\%$ ), and are calculated according to the well-known equation:

$$\Phi_{\text{overall}} = \frac{n^2 A_{\text{ref}} I}{n_{\text{ref}}^2 A I_{\text{ref}}} \Phi_{\text{ref}}$$

where *n*, *A*, and *I* denote the refractive index of solvent, and the absorbance at the excitation wavelength, and the area of the emission spectrum respectively.  $\Phi_{\text{ref}}$  represents the quantum yield of the standard [Yb(TTA)<sub>3</sub>(H<sub>2</sub>O)<sub>2</sub>] solution. The subscript ref denotes the reference, and the absence of a subscript implies an unknown sample. The estimated errors are  $\pm 10\%$  for the quantum yields and  $\pm 5\%$  for the lifetime determinations.

### Computational Details

DFT geometry optimizations and TD-DFT excitation energy calculations of two ligands were carried out with the Gaussian 09 package.<sup>25</sup> In both cases, the B3LYP/def2-TZVP basis set was used. The first 50 mono-electronic excitations were calculated. All calculations were done in the gas phase, and geometry optimizations were performed with no symmetry restraints.

The ground state geometries of two ytterbium complexes **1** and **2** were optimized by calculations using LUMPAC<sup>26</sup> with a Sparkle/PM6 model implemented in the MOPAC 2016 software. The keywords used in the calculation reported here were PM6, PRECISE, BFGS, GNORM = 0.25, GEO-OK, SCFCRT = 1.D-

10 (to increase the SCF convergence criterion) and XYZ (for Cartesian coordinates).  
DOI: 10.1039/C9DT00614A

## Synthetic procedures

### 4,4'-diacetyl triphenylamine

To a stirred solution of triphenylamine (0.98 g, 4.00 mmol) in 30 mL dry nitrobenzene, acetyl chloride (0.66 g, 8.40 mmol) and anhydrous AlCl<sub>3</sub> (1.12 g, 8.40 mmol) dissolved in 20 mL dry nitrobenzene were added dropwisely. The reaction was carried out at room temperature for 12 hours and then poured into 150 mL ice-water. The resulting organic layers were combined and dried by anhydrous Na<sub>2</sub>SO<sub>4</sub>. The solution was concentrated under reduced pressure to give the crude product, which was purified by recrystallization from n-hexane to afford a yellow bulk crystals (1.04 g, 79%). Anal. Calc. for C<sub>22</sub>H<sub>19</sub>NO<sub>2</sub> (329.14): C, 80.22; H, 5.81; N, 4.25; O, 9.71. Found: C, 80.13; H, 5.88; N, 4.21; O, 9.78. <sup>1</sup>H NMR (DMSO-*d*<sub>6</sub> 400 MHz)  $\delta$  3.31 (s, 6H), 7.06 (d, *J* = 8.8 Hz, 4H), 7.16 (d, *J* = 7.4 Hz, 2H), 7.27 (t, *J* = 7.4 Hz, 2H), 7.44 (t, *J* = 8.9 Hz, 1H), 7.90 (d, *J* = 8.4 Hz, 4H). EI-MS *m/z* 329.14 M<sup>+</sup>.

### 4,4'-di(4,4'-trifluoro-1,3-dioxobutyl)-triphenylamine (L<sup>1</sup>)

A mixture of sodium methoxide (1.08 g, 20 mmol) and ethyl trifluoroacetate (2.84 g, 20.00 mmol) in 40 mL dry DME (ethylene glycol dimethyl ether) was stirred for 10 min, followed by the addition of 4,4'-diacetyl triphenylamine (2.77 g, 8.40 mmol), which was further stirred at room temperature for 24 h (Scheme 1). The resulting mixture was poured into 100 mL ice-water and acidified to pH = 2–3 using hydrochloric acid (2.0 M), the resulting orange precipitate was filtered and dried in vacuum. Recrystallization from acetone gave orange needle crystals (4.16 g, 95%). Anal. Calc. for C<sub>26</sub>H<sub>22</sub>F<sub>6</sub>N<sub>2</sub>O<sub>4</sub> (521.11): C, 59.89; H, 3.29; N, 2.69; O, 12.27. Found: C, 59.84; H, 3.34; N, 2.66; O, 12.25. <sup>1</sup>H NMR (DMSO-*d*<sub>6</sub> 400 MHz)  $\delta$  6.71 (s, 2H), 7.15 (d, *J* = 8.8 Hz 2H), 7.21 (d, *J* = 7.6 Hz, 2H), 7.34 (t, *J* = 7.5 Hz, 1H), 7.46 (t, *J* = 7.8 Hz, 2H), 7.95 (d, *J* = 8.8 Hz, 4H), 15.4 (br, 2H). ESI-MS *m/z* 522.11 [M + H]<sup>+</sup>

### 4-(*N,N*-Dimethylamino)-4',4''-diacetyltriphenylamine

4-(*N,N*-Dimethylamino)phenyl diphenylamine was firstly prepared according to the process described in the literature.<sup>27</sup> In a three necked flask were placed 4-bromo-*N,N*-dimethylaniline (9.00 g, 0.045 mol), diphenylamine (7.61 g, 0.045 mol), sodium-*t*-butoxide (6.48 g, 0.068 mol), Pd(OAc)<sub>2</sub> (0.20 g, 0.90 mmol), tri(*tert*-butyl)phosphine (0.55 g, 2.70 mmol) and 300 mL toluene, and the mixture was stirred at 90 °C for 18 h. After completion of the reaction, the mixture was cooled to room temperature, then rinsed with saturated NH<sub>4</sub>Cl (2.0 mL). The resulting aqueous phase was extracted with CH<sub>2</sub>Cl<sub>2</sub> (10 mL  $\times$  3). The organic layers were combined and dried over anhydrous MgSO<sub>4</sub>. The solution was concentrated under reduced pressure to give the crude product, which was purified by column chromatography (silica, 5% EtOAc in hexanes) to give the product as a white solid (11.02 g, 85%).

4-(*N,N*-Dimethylamino)-4',4''-diacetyltriphenylamine was synthesized according to the processes described for the isolation of 4,4'-diacetyl triphenylamine by utilizing 1.15 g (4.00 mmol) of 4-(*N,N*-Dimethylamino)phenyl diphenylamine, 1.02 g (10.00 mmol) of acetic anhydride and 2.67 g (20.00 mmol) of AlCl<sub>3</sub>.

Purification by recrystallization from n-hexane afford a yellow bulk crystals (1.22 g, 82%). Anal. Calc. for  $C_{24}H_{24}N_2O_2$  (372.18): C, 77.39; H, 6.50; N, 7.52; O, 8.59. Found: C, 77.34; H, 6.58; N, 7.58; O, 8.55.  $^1H$  NMR ( $CDCl_3$ )  $\delta$  2.57(s, 6H), 3.01 (s, 6H), 6.76(d,  $J = 9.0$  Hz, 2H), 7.06 (d,  $J = 8.8$  Hz, 2H), 7.12 (d,  $J = 8.8$  Hz, 4H), 7.86 (d,  $J = 8.8$  Hz, 4H). ESI-MS  $m/z$  373.18  $[M + H]^+$ .

#### 4-(N,N-dimethylamino)-4',4''-di(4,4',4''-trifluoro-1,3-dioxobutyl)-triphenylamine ( $L^2$ )

A mixture of sodium methoxide (1.08 g, 20 mmol) and ethyl trifluoroacetate (2.84 g, 20.00 mmol) in 40 mL dry DME (ethylene glycol dimethyl ether) were stirred for 10 min, followed by the addition of 4-(N,N-Dimethylamino)-4',4''-diacetyltriphenylamine (3.13 g, 8.40 mmol), which was further stirred at room temperature for 24 h. The resulting mixture was poured into 100 mL ice-water and acidified to pH = 2–3 using hydrochloric acid (2.0 M), the resulting orange precipitate was filtered and dried in vacuum. Recrystallization from acetone gave brown needle crystals (2.80 g, 59.0%). Anal. Calc. for  $C_{28}H_{22}F_6N_2O_4$  (564.14): C, 59.58; H, 3.93; N, 4.96; O, 11.34. Found: C, 59.55; H, 4.02; N, 4.92; O, 11.57.  $^1H$  NMR ( $CDCl_3$ )  $\delta$  3.03 (s, 6H), 6.49 (s, 2H), 6.76(d,  $J = 9.0$  Hz, 2H), 7.06 (d,  $J = 9.0$  Hz, 2H), 7.18 (d,  $J = 8.8$  Hz, 4H), 7.86 (d,  $J = 8.8$  Hz, 4H), 15.46 (br, 2H). ESI-MS  $m/z$  565.14  $[M + H]^+$ .

#### Synthesis of $(HNEt_3)_2[M_2L^1_4]$ and $(HNEt_3)_2[M_2L^2_4]$

$L^1$  and  $L^2$  (0.18 mmol) and triethylamine (36.00 mg, 0.36 mmol) were dissolved in 10 mL  $CH_3CN$ . To this solution cooled to room temperature,  $MCl_3 \cdot 6H_2O$  ( $M = Yb, Gd$  and  $Y$ ; 0.090 mmol) in 10 mL  $CH_3CN$  were added dropwisely to the solution and stirred for 24 h (Scheme 1). The precipitate formed after the addition of water was filtered, and washed successively with  $H_2O$  ( $2 \times 10$  mL),  $CH_3OH$  ( $2 \times 10$  mL) and diethyl ether ( $2 \times 10$  mL), then dried under vacuum to give the desired products.

$(HNEt_3)_2[Yb_2(L^1)_4]$  (**1**) Yield: 82%. Anal. Calc. for  $C_{116}H_{92}F_{24}N_6O_{16}Yb_2$  (2627.50): C, 53.01; H, 3.53; N, 3.20; O, 9.74. Found: C, 53.23; H, 3.66; N, 3.17; O, 9.71. ESI-MS:  $m/z = 1212.1161 [Yb_2(L^1)_4]^{2-}$ .

$(HNEt_3)_2[Yb_2(L^2)_4]$  (**2**) Yield: 85%. Anal. Calc. For  $C_{124}H_{112}F_{24}N_{10}O_{16}Yb_2$  (2799.67): C, 53.18; H, 4.03; N, 5.00; O, 9.14. Found: C, 53.20; H, 4.15; N, 5.08; O, 9.13. ESI-MS:  $m/z = 1298.2021 [Yb_2(L^2)_4]^{2-}$ .

$(HNEt_3)_2[Gd_2(L^1)_4]$  (**3**) Yield: 82%. Anal. Calc. For  $C_{116}H_{92}F_{24}N_6O_{16}Gd_2$  (2599.47): C, 53.66; H, 3.57; N, 3.24; O, 9.86. Found: C, 53.62; H, 3.61; N, 3.29; O, 9.81. ESI-MS:  $m/z = 1195.4380 [Gd_2(L^1)_4]^{2-}$ .

$(HNEt_3)_2[Gd_2(L^2)_4]$  (**4**) Yield: 81%. Anal. Calc. For  $C_{124}H_{112}F_{24}N_{10}O_{16}Gd_2$  (2771.64): C, 53.79; H, 4.08; N, 5.06; O, 9.25. Found: C, 53.65; H, 4.29; N, 5.15; O, 9.21. ESI-MS:  $m/z = 1283.1941 [Gd_2(L^2)_4 + H]^{2-}$ .

$(HNEt_3)_2[Y_2(L^1)_4]$  (**5**) Yield: 82%. Anal. Calc. For  $C_{116}H_{92}F_{24}N_6O_{16}Y_2$  (2459.43): C, 56.64; H, 3.77; N, 3.42; O, 10.41. Found: C, 56.66; H, 3.82; N, 3.44; O, 10.35. ESI-MS:  $m/z = 1127.0832 [Y_2(L^1)_4]^{2-}$ .

$(HNEt_3)_2[Y_2(L^2)_4]$  (**6**) Yield: 85%. Anal. Calc. For  $C_{124}H_{112}F_{24}N_{10}O_{16}Y_2$  (2631.60): C, 56.58; H, 4.29; N, 5.32; O, 9.73. Found: C, 56.62; H, 4.33; N, 5.28; O, 9.68. ESI-MS:  $m/z = 1213.1695 [Y_2(L^2)_4]^{2-}$ .

## Conflicts of interest

There are no conflicts to declare.

View Article Online

DOI: 10.1039/C9DT00614A

## Acknowledgements

This work is financially supported by the National Natural Science Foundation of China (Nos. 51773054 & 51872077). We also thank the Key Laboratory of Functional Inorganic Material Chemistry, Ministry of Education, P. R. China for supporting this work.

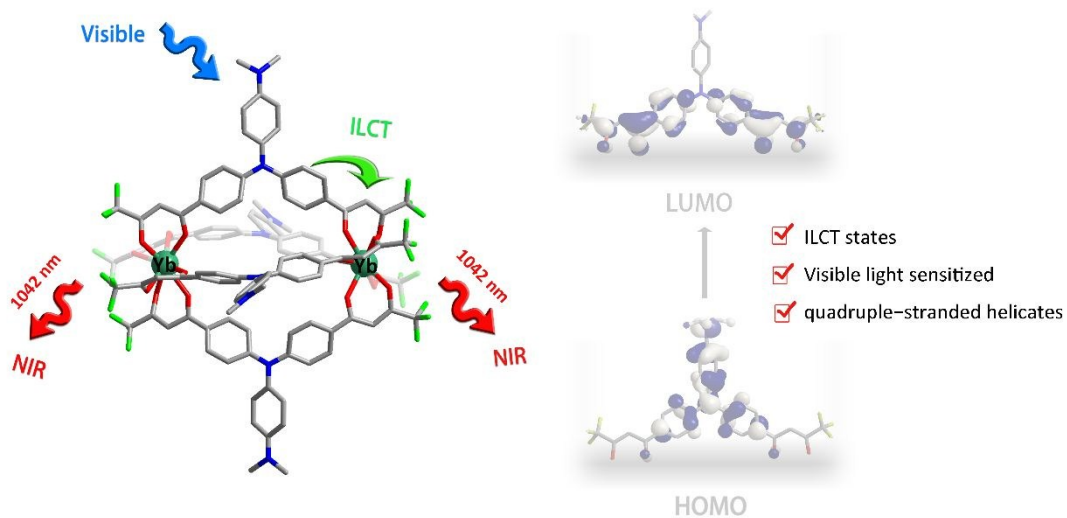
## References

- (a) M. T. Kaczmarek, M. Zabiszak, M. Nowak and R. Jastrzab, *Coord. Chem. Rev.*, 2018, **370**, 42–54; (b) M. Sy, A. Nonat, N. Hildebrandt and L. J. Charbonnière, *Chem. Comm.*, 2016, **52**, 5069–5208; (c) K. Dong, E. Ju, N. Gao, Z. Wang, J. Ren and X. Qu, *Chem. Comm.*, 2016, **52**, 5312–5315; (d) Q. F. Li, X. D. Du, L. Jin, M. M. Hou, Z. L. Wang and J. H. Hao, *J. Mater. Chem. C*, 2016, **4**, 3195–3201; (e) A. J. Amoroso and S. J. A. Pope, *Chem. Soc. Rev.*, 2015, **44**, 4723–4742; (f) T. Zhang, X. Zhu, C. C. W. Cheng, W.-M. Kwok, H.-L. Tam, J. Hao, D. W. J. Kwong, W.-K. Wong, K.-L. Wong, *J. Am. Chem. Soc.*, 2011, **133**, 20120–20122.
- (a) S. V. Eliseeva and J.-C. G. Bünzli, *Chem. Soc. Rev.*, 2010, **39**, 189–227; (b) J.-C. G. Bünzli, *Chem. Rev.*, 2010, **110**, 2729–2755; (c) Y. Ning, J. Tang, Y.-W. Liu, J. Jing, Y. Sun, J.-L. Zhang, *Chem. Sci.*, 2018, **9**, 3742–3753; (d) J.-X. Zhang, H. Li, C.-F. Chan, R. Lan, W.-L. Chan, G.-L. Law, W.-K. Wong, K.-L. Wong, *Chem. Comm.*, 2012, **48**, 9646–9648.
- (a) L. Armelao, S. Quici, F. Barigletti, G. Accorsi, G. Bottaro, M. Cavazzini and E. Tondello, *Coord. Chem. Rev.*, 2010, **254**, 487–505; (b) D. A. Galico, M. G. Lahoud, M. R. Davalos, R. C. G. Frem, T. F. C. Fraga-Silva, J. Venturini, M. S. P. Arruda, G. Bannach, *J. Inorg. Biochem.*, 2014, **140**, 160–166; (c) Y. Ning, Y.-W. Liu, Y.-S. Meng and J.-L. Zhang, *Inorg. Chem.*, 2018, **57**, 1332–1341.
- (a) W. Huang, D. Wu, D. Guo, X. Zhu, C. He, Q. Meng and C. Duan, *Dalton Trans.*, 2009, 2081–2084; (b) C.-N. Ko, G. Li, C.-H. Leung, D.-L. Ma, *Coord. Chem. Rev.*, 2019, **381**, 79–103; (c) J. Zhou, J. L. Leño Jr., Z. Liu, D. Jin, K.-L. Wong, R.-S. Liu and J.-C. G. Bünzli, *Small*, 2018, **14**, 1801882(1–29); (d) N. Souri, P. Tian, C. Platas-Iglesias, K.-L. Wong, A. Nonat and L. J. Charbonnière, *J. Am. Chem. Soc.*, 2017, **139**, 1456–1459.
- (a) J.-C. G. Bünzli, *Coord. Chem. Rev.*, 2015, **293**, 19–47; (b) S. Faulkner, L. S. Natrajan, W. S. Perry and D. Sykes, *Dalton Trans.*, 2009, 3890–3899.
- (a) S. S. Zhou, X. Xue, J. Wang, Y. Dong, B. Jiang, D. Wei, M. L. Wan, Y. Jia, *J. Mater. Chem.*, 2012, **22**, 22774–22780; (b) L. Aboshyan-Sorgho, M. Cantuel, S. Petoud, A. Hauser and C. Piguet, *Coord. Chem. Rev.*, 2012, **256**, 1644–1663; (c) M. Li, S. Gul, D. Tian, E. Zhou, Y. Wang, Y. Han, L. Yin and L. Huang, *Dalton Trans.*, 2018, **47**, 12868–12872.
- (a) V. A. Ilichev, L. I. Silantjeva, A. N. Yablonskiy, B. A. Andreev, R. V. Rumyantsev, G. K. Fukin and M. N. Bochkarev, *Dalton Trans.*, 2019, **48**, 1060–1066; (b) F. Artizzu, F. Quochi, L. Marchi, R. F. Correia, M. Saba, A. Serpe, A. Mura, M. L. Mercuri, G. Bongiovanni and P. Deplano, *Chem. – Eur. J.*, 2015, **21**, 3882–3885.
- (a) C.-L. Liu, R.-L. Zhang, C.-S. Lin, L.-P. Zhou, L.-X. Cai, J.-T. Kong, S.-Q. Yang, K.-L. Han and Q.-F. Sun, *J. Am. Chem. Soc.*, 2017, **139**, 12474–12479; (b) W.-S. Lo, W.-T. Wong and G.-L. Law, *RSC Adv.*, 2016, **6**, 74100–74109; (c)

- Y.-X. Zhu, Z.-W. Wei, M. Pan, H.-P. Wang, J.-Y. Zhang and C.-Y. Su, *Dalton Trans.*, 2016, **45**, 943–950; (d) A. D'Aléo, F. Pointillart, L. Ouahab, C. Andraud and O. Maury, *Coord. Chem. Rev.*, 2012, **256**, 1604–1620; (e) N. M. Shavaleev, R. Scopelliti, F. Gumy and J.-C.G. Bünzli, *Eur. J. Inorg. Chem.*, 2008, 1523–1529; (f) A. D'Aléo, A. Picot, A. Beeby, J. A. G. Williams, B. Le Guennic, C. Andraud and O. Maury, *Inorg. Chem.*, 2008, **47**, 10258–10268.
- 9 F. Pointillart, A. Bourdolle, T. Cauchy, O. Maury, Y. Le Gal, S. Golhen, O. Cadour and L. Ouahab, *Inorg. Chem.*, 2012, **51**, 978–984.
- 10 F. Pointillart, T. Cauchy, O. Maury, Y. Le Gal, S. Golhen, O. Cadour and L. Ouahab, *Chem. – Eur. J.*, 2010, **16**, 11926–11941.
- 11 (a) X.-Z. Li, L.-P. Zhou, L.-L. Yan, D.-Q. Yuan, C.-S. Lin and Q.-F. Sun, *J. Am. Chem. Soc.*, 2017, **139**, 8237–8244; (b) A. K. Mondal, H. S. Jena, A. Malviya and S. Konar, *Inorg. Chem.*, 2016, **55**, 5237–5244; (c) J. L., Greenfield, E. W. Evans, D. Di Nuzzo, M. Di Antonio, R. H. Friend and J. R. Nitschke, *J. Am. Chem. Soc.*, 2018, **140**, 10344–10353; (d) M. Estrader, J. S. Uber, L. A. Barrios, J. Garcia, P. Lloyd-Williams, O. Roubeau, S. J. Teat and G. Aromí, *Angew. Chem. Int. Ed.*, 2017, **56**, 1–7.
- 12 (a) D. Zare, Y. Suffren, H. Nozary, A. Hauser and C. Piguet, *Angew. Chem. Int. Ed.*, 2017, **56**, 14612–14617; (b) L. Babel, L. Guénée, C. Besnard, S. V. Eliseeva, S. Petoud and C. Piguet, *Chem. Sci.*, 2018, **9**, 325–335; (c) L. Babel, T. N. Y Hoang, L. Guénée, C. Besnard, T. A. Wesolowski, M. Humbert-Droz and C. Piguet, *Chem. – Eur. J.*, 2016, **22**, 8113–8123; (d) L. Aboshyan-Sorgho, H. Nozary, A. Aebischer, J.-C. G. Bünzli, P.-Y. Morgantini, K. R. Kittilstved, A. Hauser, S. V. Eliseeva, S. Petoud and C. Piguet, *J. Am. Chem. Soc.*, 2012, **134**, 12675–12684; (e) P. E. Ryan, L. Guénée and C. Piguet, *Dalton Trans.*, 2013, **42**, 11047–11055; (f) C. Piguet and J.-C. G. Bünzli, *Handbook on the Physics and Chemistry of Rare Earths*, Elsevier: Amsterdam, 2010; Vol. 40, Chapter 247, pp 301–553.
- 13 (a) B. Li, H. Li, P. Chen, W. Sun, C. Wang, T. Gao and P. Yan, *Dalton Trans.*, 2016, **45**, 11459–11470; (b) B. Li, H. Li, P. Chen, W. Sun, C. Wang, T. Gao and P. Yan, *Phys. Chem. Chem. Phys.*, 2015, **17**, 30510–30517; (c) H. Li, P. Yan, P. Chen, W. Yan, H. Xu and G. Li, *Dalton Trans.*, 2012, **41**, 900–907.
- 14 (a) B. N. Ghosh, F. Topić, P. K. Sahoo, P. Mal, J. Linnera, E. Kalenius, H. M. Tuononen and K. Rissanen, *Dalton Trans.*, 2015, **44**, 254–267; (b) X.-Y. Wang, A. Del Guerso and R. H. Schmehl, *Chem. Comm.*, 2002, 2344–2345.
- 15 C. Reichardt, *Chem. Rev.*, 1994, **94**, 2319–2358.
- 16 (a) R. F. Ziessel, G. Ulrich, L. Charbonnière, D. Imbert, R. Scopelliti and J.-C. G. Bünzli, *Chem. – Eur. J.*, 2006, **12**, 5060–5067; (b) K. Mason, A. C. Harnden, C. W. Patrick, A. W. J. Poh, A. S. Batsanov, E. A. Suturina, M. Vonci, E. J. L. McInnes, N. F. Chilton and D. Parker, *Chem. Commun.*, 2018, **54**, 8486–8489.
- 17 M. P. Tsvirko, S. B. Meshkova, V. Y. Venchikov and D. V. Bol'shoi, *Opt. Spectrosc. (Engl. Transl.)*, 1999, **87**, 866–870.
- 18 (a) J. Salaam, L. Tabti, S. Bahamyirou, A. Lecointre, O. H. Alba, O. Jeannin, F. Camerel, S. Cianférani, E. Bentouhami, A. M. Nonat and L. J. Charbonnière, *Inorg. Chem.*, 2018, **57**, 6095–6106; (b) K. Jinnai, R. Kabe and C. Adachi, *Chem. Commun.*, 2017, **53**, 5457–5460; (c) A. W. Woodward, A. Frazer, A. R. Morales, J. Yu, A. F. Moore, A. D. Campiglia, E. V. Jucov, T. V. Timofeeva and K. D. Belfield, *Dalton Trans.*, 2014, **43**, 16626–16639; (d) H. Wei, G. Yu, Z. Zhao, Z. Liu, Z. Bian and C. Huang, *Dalton Trans.*, 2013, **42**, 8951–8960.
- 19 (a) N. M. Shavaleev, S. V. Eliseeva, R. Scopelliti and J.-C. G. Bünzli, *Inorg. Chem.*, 2014, **53**, 5171–5178; (b) M. H. V. Werts, R. T. F. Jukes and J. W. Verhoeven, *Phys. Chem. Chem. Phys.*, 2002, **4**, 1542–1548; (c) K. Binnemans, R. V. Deun, C. Görrler-Walrand, S. R. Collinson, F. Martin, D. W. Bruce and C. Wickleder, *Phys. Chem. Chem. Phys.*, 2000, **2**, 3753–3757.
- 20 (a) E. Kasprzycka, V. A. Trush, V. M. Amirkhanov, L. Jerzykiewicz, O. L. Malta, J. Legendziewicz and P. Gawryszewska, *Chem. – Eur. J.*, 2017, **23**, 1318–1330; (b) J. Andres and A.-S. Chauvin, *Phys. Chem. Chem. Phys.*, 2013, **15**, 15981–15994.
- 21 (a) T. Zhu, P. Chen, H. Li, W. Sun, T. Gao and P. Yan, *Phys. Chem. Chem. Phys.*, 2015, **17**, 16136–16144; (b) J. Leng, H. Li, P. Chen, W. Sun, T. Gao and P. Yan, *Dalton Trans.*, 2014, **43**, 12228–12235.
- 22 (a) M. Pan, B.-B. Du, Y.-X. Zhu, M.-Q. Yue, Z.-W. Wei and C.-Y. Su, *Chem. – Eur. J.*, 2016, **22**, 2440–2451; (b) W.-S. Lo, J. Zhang, W.-T Wong and G.-L. Law, *Inorg. Chem.*, 2015, **54**, 3725–3727.
- 23 (a) A. Chandra, K. Singh, S. Singh, S. Sivakumar and A. K. Patra, *Dalton Trans.*, 2016, **45**, 494–497; (b) L.-Y. Zhang, Y.-J. Hou, M. Pan, L. Chen, Y.-X. Zhu, S.-Y. Yin, G. Shao and C.-Y. Su, *Dalton Trans.*, 2015, **44**, 15212–15219.
- 24 H. Xiang, J. Cheng, X. Ma, X. Zhou and J. J. Chruma, *Chem. Soc. Rev.*, 2013, **42**, 6128–6185.
- 25 M. J. Frisch, G. W. Trucks, H. B. Schlegel, G. E. Scuseria, M. A. Robb, J. R. Cheeseman, G. Scalmani, V. Barone, B. Mennucci, G. A. Petersson, H. Nakatsuji, M. Caricato, X. Li, H. P. Hratchian, A. F. Izmaylov, J. Bloino, G. Zheng, J. L. Sonnenberg, M. Hada, M. Ehara, K. Toyota, R. Fukuda, J. Hasegawa, M. Ishida, T. Nakajima, Y. Honda, O. Kitao, H. Nakai, T. Vreven, J. A. Montgomery Jr., J. E. Peralta, F. Ogliaro, M. Bearpark, J. J. Heyd, E. Brothers, K. N. Kudin, V. N. Staroverov, T. Keith, R. Kobayashi, J. Normand, K. Raghavachari, A. Rendell, J. C. Burant, S. S. Iyengar, J. Tomasi, M. Cossi, N. Rega, J. M. Millam, M. Klene, J. E. Knox, J. B. Cross, V. Bakken, C. Adamo, J. Jaramillo, R. Gomperts, R. E. Stratmann, O. Yazyev, A. J. Austin, R. Cammi, C. Pomelli, J. W. Ochterski, R. L. Martin, K. Morokuma, V. G. Zakrzewski, G. A. Voth, P. Salvador, J. J. Dannenberg, S. Dapprich, A. D. Daniels, O. Farkas, J. B. Foresman, J. V. Ortiz, J. Cioslowski and D. J. Fox, EM64L Gaussian 09, Revision D.01, Gaussian, Inc., Wallingford CT, 2013.
- 26 J. D. L. Dutra, T. D. Bispo and R. O. Freire, *J. Comput. Chem.*, 2014, **35**, 772–775.
- 27 F. E. Goodson, S. I. Hauck and J. F. Hartwig, *J. Am. Chem. Soc.* 1999, **121**, 7527–7539.

## Visible light sensitized near-infrared luminescence of ytterbium via ILCT states in quadruple-stranded helicates

Zihan Zhang, Yanyan Zhou, Hongfeng Li,\* Ting Gao and Pengfei Yan\*



The quadruple-stranded helicates show visible light sensitized near-infrared luminescence of ytterbium via ILCT states.